Mesoscale organization of metal nanocrystals*

G. U. Kulkarni[‡], P. John Thomas, and C. N. R. Rao

Chemistry and Physics of Materials Unit, Jawaharlal Nehru Center for Advanced Scientific Research, Jakkur, Bangalore 560 064, India

Abstract: Nanocrystals of metals covered by alkanethiols organize themselves in two-dimensional arrays. We discuss such arrays of metal nanocrystals at length, with focus on the dependence of the structure and the stability of the arrays on the particle diameter and the distance between the particles. Three-dimensional superstructures of metal nanocrystals obtained by the use of alkanedithiols are examined. These ordered two- and three-dimensional structures of thiolized metal nanocrystals are good examples of mesoscale self-assembly. The association of metal nanocrystals to give rise to giant clusters with magic nuclearity provides an even more graphic demonstration of mesoscale self-assembly.

INTRODUCTION

A metal nanocrystal is a tiny chunk of the bulk measuring a few nanometers with a finite number of metal atoms in it. The forces that govern the nanocrystal structure, however, are different in many ways. Surface tension, for example, plays an important role [1] because in a nanocrystal, a large fraction of atoms are present at the surface. Consequently, the structure of a metal nanocrystal may exhibit features unknown in an extended lattice, such as a five-fold symmetry [2]. Nanocrystals with a specific number of atoms (nuclearity) are bequeathed with special stability [3]. For nanocrystals of cubic close-packed metals, the numbers 13, 55, 147, 309, and 561 stand for magic nuclearities corresponding to the closure of 1, 2, 3, 4, and 5 shells, respectively. A schematic illustration of magic nuclearity nanocrystals is shown in Fig. 1. Unprotected nanocrystals are unstable by nature and tend to coalesce with other nanocrystals. Therefore, the surface of a nanocrystal needs to be passivated with ligands such as long-
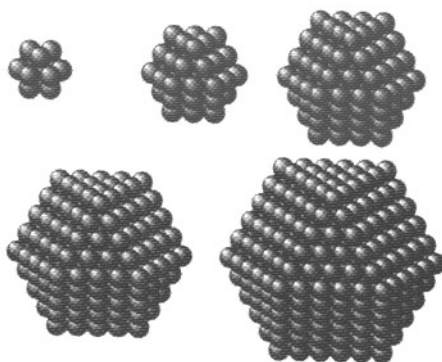

Fig. 1 Metal nanocrystals in closed-shell configurations with magic number of atoms.

[‡]Corresponding author

chain fatty acids, thiols, amines, and polymers to prevent aggregation. The ligated nanocrystals are dispersible in various solvents. Magic nuclearity Pd nanocrystals passivated with poly(vinylpyrrolidone) (PVP) have been prepared in this laboratory. The scanning tunneling micrograph in Fig. 2 shows a few Pd_{561} nanocrystals. Its internal structure is revealed by high-resolution transmission electron microscopy.

Size-dependent—chemical, magnetic, and electronic—properties of the metal nanocrystals owing to quantum confinement of the electronic states [4–6] are interesting to study. In the case of metal nanocrystals, the electronic energy levels are not continuous as in bulk materials, but discrete. An approximate idea of the average electronic energy level spacing of successive quantum levels, δ can be obtained using Kubo's theory [4]. For an individual silver nanocrystal of 3-nm diameter containing approximately 1000 silver atoms, the value of δ would be 5–10 meV. Since the thermal energy at room temperature, $kT \cong 25$ meV, a 3-nm particle would be metallic ($kT > \delta$). At low temperatures, however, the level spacings, especially in small particles, may become comparable to kT, rendering them nonmetallic [4]. Such changes can be followed directly by scanning tunneling spectroscopy (STS) on individual particles [7]. A systematic STS study of Pd, Ag, Cd, and Au nanoparticles of varying sizes deposited on a graphite substrate revealed that small particles of ≤1-nm diameter are in fact nonmetallic! It appears that the size-induced metal–insulator transition in metal nanocrystals occurs in the range of 1–2 nm diameter or 300 ± 100 atoms [4].

An added dimension to this area of research is the mesoscale self-assembly of nanocrystals. Cooperative assemblies of ligated metal [8] and semiconductor nanocrystals [9], as well as of colloidal polymer spheres seem to occur through the mediation of electrostatic and capillary forces [10,11]. The ability to engineer such assemblies extends the reach of current lithographic techniques and holds promise for a new generation of electronics of the nano-world. In this context, synthesis and programmed assembly of metal nanocrystals assumes significance [8]. In this article, we examine the structure and stability of mesoscopic organizations of nanocrystals obtained using alkanethiols and PVP as surfactants. It is shown that nanocrystals covered with thiols form ordered arrays, while those protected with the polymer self-aggregate into giant clusters. Interestingly, the giant clusters exhibit magic nuclearity with respect to the number of nanocrystals.
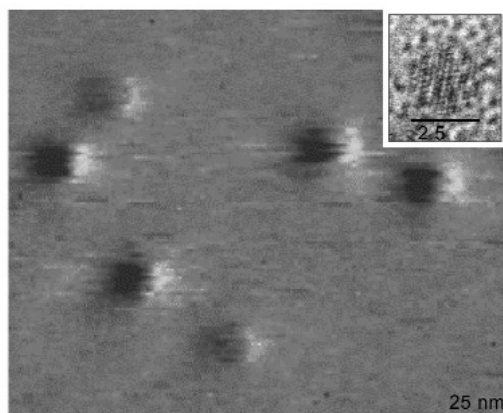

Fig. 2 STM image of polymer-coated Pd_{561} nanocrystals. The nanocrystals are seen as fluffy balls against plane background of the graphite substrate. The inset shows a high-resolution electron micrograph (HRTEM) of an individual nanocrystal. We see the characteristic 11 [111] fringes in the icosahedral shape measuring 2.5 nm. The diameter estimated from STM is ~3.4 nm, the difference being due to the ligand shell.

ORDERED ASSEMBLIES

Surfactant molecules that self-assemble on metal surfaces have proved to be the best means of obtaining ordered arrays of nanocrystals [8]. The way in which the nanocrystals organize themselves depends critically on the metal core diameter, the nature of the ligand, substrate, and even the dispersive medium used [12]. Thiolized (alkanethiol-capped) nanocrystals readily arrange into two-dimensional arrays on removal of the solvent [8]. Using suitable methods, they can also be put into one-dimensional organization in the form of strings or assembled in a stepwise fashion in a three-dimensional superlattice. The different possibilities of organizing nanocrystals are schematically illustrated in Fig. 3.

The effect of the thiol chain length on nanocrystal organization is illustrated in Fig. 4 in the case of Pd nanocrystals with mean diameter of 4.5 nm. The formation of an ordered two-dimensional nanocrystal array seems to depend critically on the size of the metal nanocrystal and the extent of interdigitation of hydrocarbon chains from neighboring nanocrystals. The nanocrystals were initially prepared with PVP as the capping agent, and subsequently the capping agent was replaced with alkanethiols of varying chain lengths adopting a procedure developed in our laboratory [13–15]. The butanethiol-coated nanocrystals form agglomerates, 20–40 nm in size, with little internal order as shown in Fig. 4a. In many regions, the particles do not show distinct boundaries. Longer-chain thiols give rise to close-packed arrays (Figs. 4b, 4c, and 4d) spread over micron-sized areas. The contrasting behavior of butanethiol (Fig. 4a) is clearly due to its short chain length. The role of the thiol chain length becomes more evident when we closely examine the organizations in Figs. 4b, 4c, and 4d. The 4.5-nm
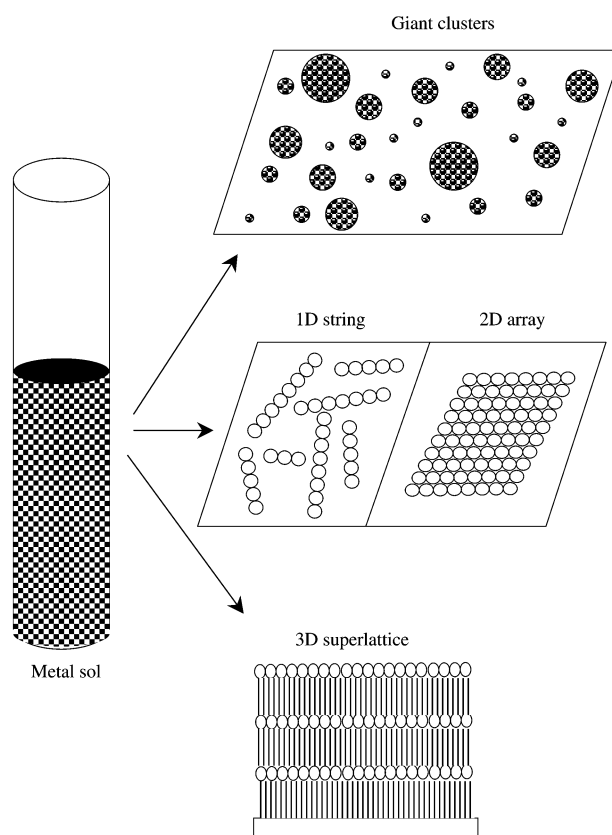

Fig. 3 Schematic illustration of the various metal nanocrystal organizations.
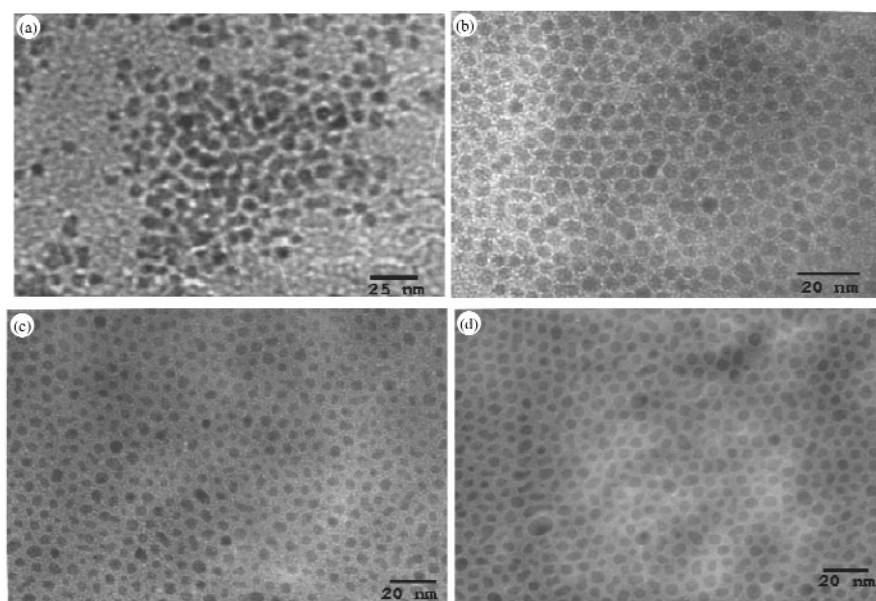
Fig. 4 TEM micrographs showing Pd nanocrystals of mean diameter 4.5 nm organized into two-dimensional lattices using different thiols: (a) butanethiol, (b) octanethiol, (c) dodecanethiol, and (d) hexadecanethiol.

nanocrystals covered with octanethiol form a honeycomb lattice (Fig. 4b) in which we observe short-range order limited to three or four hexagons of nanocrystals. The packing is facilitated in many places by a curved arrangement of the nanocrystals. On the other hand, the 4.5-nm sol derivatized with dode-canethiol and hexadecanethiol, crystallize in close-packed structures as shown in Figs. 4c and 4d, respectively, resembling the jammed arrangements of polydisperse spheroids [16]. An examination of the extent of thiol interdigitation (interpenetration of the molecular chains present at the surface of the nanocrystals) reveals some interesting aspects of the two-dimensional organizations. Assuming a fully extended all-trans conformation of the thiol molecule inclined at 30° on the particle surface, the projected chain lengths (l) are ~ 0.8, 1.2, 1.7, and 2.1 nm for the butane-, octane-, dodecane- and hexade-canethiol, respectively [17]. The values of interdigitation for octane, dodecane, and hexadecane thiols are, therefore, 30 %, 18 %, and 24 % of the respective chain lengths.

The results obtained with several sets of particles and thiols clearly demonstrate that the nature of nanocrystal organization depends on both the particle diameter, d, and the thiol chain length, l. A stability diagram in terms of d and l was derived based on this study. In Fig. 5, the bright area in the middle is the most favorable d/l regime, corresponding to extended close-packed organizations of nanocrystals such as those illustrated in Figs. 4b–4d. The d/l values in this area are in the range, 1.5–3.8. The area shaded dark in Fig. 5 includes the d/l regime, giving rise to various short-range aggregations, formed when the particles are small and the chain length is large, or vice versa.

We sought to understand the nature and stability of the two-dimensional arrays of thiolized Pd nanocrystals in terms of the particle diameter, d, and the chain length, l. We have made use of a soft-sphere model, taking the interparticle interaction into consideration. Accordingly, a ligated nanocrystal allows for penetration of the ligand shell up to its hard sphere limit. In this model, the total potential energy, E, is considered to be a result of two types of forces between the nanocrystals,

$$E = E_{steric} + E_{vdW} \tag{1}$$

C_n *(l nm)*

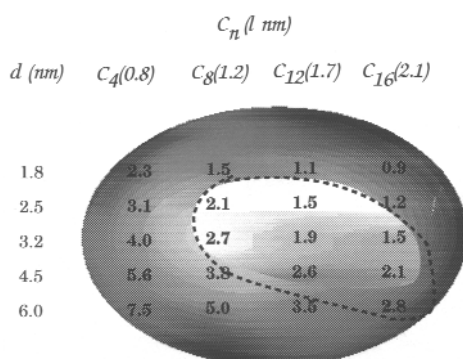| *d (nm)*	*C_4(0.8)*	*C_8(1.2)*	*C_{12}(1.7)*	*C_{16}(2.1)*
1.8	2.3	1.5	1.1	0.9
2.5	3.1	2.1	1.5	1.2
3.2	4.0	2.7	1.9	1.5
4.5	5.6	3.8	2.6	2.1
6.0	7.5	5.0	3.5	2.8

Fig. 5 The *d/l* phase diagram for Pd nanocrystals thiolized with different alkanethiols. The mean diameter, *d*, was obtained from the TEM measurements on as-prepared sols. The length of the thiol, *l*, is estimated by assuming an all-trans conformation of the alkane chain. The thiol is indicated by the number of carbon atoms, C_n. The bright area in the middle encompasses systems that form close-packed organizations of nanocrystals. The surrounding darker area includes disordered or low-order arrangements of nanocrystals. The area enclosed by the dashed line is derived from calculations from the soft-sphere model.

The van der Waals interaction due to the polarization of the metal cores constitutes the attractive term and the steric interaction between the thiol molecules on the two surfaces forms the repulsive term,

$$E_{\text{vdW}} = \frac{A}{12}\left\{\frac{d^2}{\tau^2 - d^2} + \frac{d^2}{\tau^2} + 2\ln\left(\frac{\tau^2 - d^2}{\tau^2}\right)\right\} \tag{2}$$

$$E_{\text{steric}} = \frac{50dl^2}{(\tau - d)\pi\sigma_a{}^3}kTe^{-\pi(\tau - d)} \tag{3}$$

where τ is the interparticle distance. The Hamaker constant, A, for Pd nanocrystals in toluene has been estimated to be 1.95 eV [18]. The calculated diameter of the area occupied by the thiol molecule (σ_a) on the particle surface is ~4.3 Å [19]. The total energy is attractive over a range of interparticle distances, the magnitude increasing with fall in distance. There could be a range of interparticle distances where the attractive energy from the van der Waals term exceeds the repulsive energy due to the steric factor, giving rise to net stabilization of the two-particle system. Stabilization energies (depth of the potential energy well) of 17 and 2 meV were obtained from the calculation for 4.5-nm Pd nanocrystals coated with octanethiol and dodecanethiol, respectively.

In Fig. 6, we depict the stabilization energies for *d/l* values corresponding to the experimentally investigated systems. With shorter thiol chain lengths or larger metal cores (*d/l* > 3), we observe steep potential energy wells in the range of tens of meV, possibly implying agglomeration of the particles. For *d/l* < 1.5, the two-particle system exhibits a shallow minimum with negligible stabilization, corresponding to a situation where long thiol chains shield the attractive interactions between the metal cores. An organization of this kind is influenced more by the directional property of the thiol chain resulting in lower order structures. For *d/l* values in the range ~2.0–3.0, the stabilization energies have moderate values (we show this regime by the dashed line in Fig. 5) and are comparable to the thermal energy of the nanocrystals at room temperature. This energy is perhaps just enough to bring the metal particles in the medium closer till the interaction turns repulsive. It is indeed gratifying to note that the *d/l* regime for extended organization of nanocrystals as predicted by the soft-sphere model (indicated with a dashed line in Fig. 5) matches well with that observed experimentally (the area shaded white in Fig. 5).
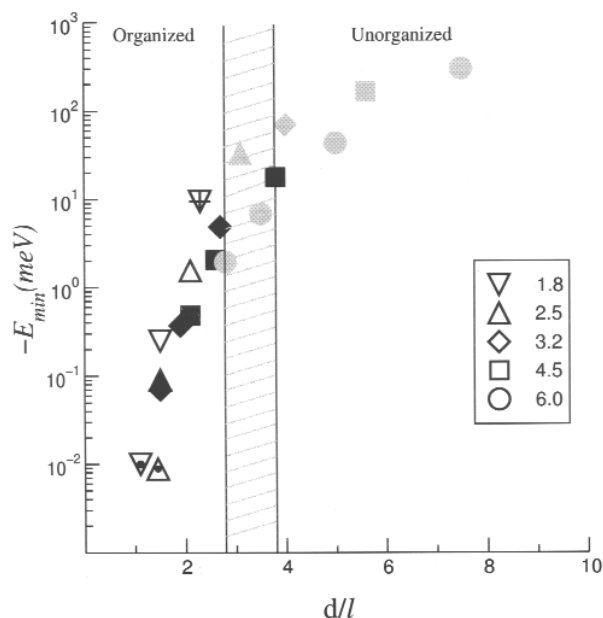
Fig. 6 Variation of the stabilization energy against *d/l* for various nanocrystal-thiol systems. The particle diameters are indicated against the corresponding symbols in the legend box. Filled, crystalline organization; plus marked, dimers, and trimers; centered, 1-D string; grey, disordered organization.

We have also investigated the two-dimensional arrays of magic nuclearity Pd_{561} and Pd_{1415} nanocrystals (five and seven, shelled respectively), stabilized by alkanethiols. In an effort to obtain arrays of magnetic metal nanocrystals, a shell of Ni was deposited on PVP-coated Pd_{561} nanocrystals adopting the procedure of Ternaishi et al. [20] followed by thiolization adopting our method. The nanocrystals so obtained consist of a Pd core and a Ni shell, as illustrated schematically in Fig. 7a. Core-shell nanocrystals, $Pd_{561}Ni_n$ (n = 38, 280, 561, 800, 1500, 3000, 4600) were prepared and thiolized by this way. Different amounts of Ni could be coated onto a Pd_{561} seed, and the magnetic moment of the obtained Pd–Ni particles scales linearly with the Ni coating. The zero-field cooled (ZFC) measurements for octanethiol-coated $Pd_{561}Ni_{1500}$ and $Pd_{561}Ni_{4500}$ nanocrystals are shown in Fig. 7b. The field-cooled measurements yielded curves overlapping with the ZFC curves. It is observed that the ratio of the measured magnetic moments ($Pd_{561}Ni_{4500}$ / $Pd_{561}Ni_{1500}$) is ~3 at all temperatures. The Pd–Ni core shell nanocrystals do not exhibit a hystersis even at 5 K (see inset of Fig. 7b). The thiolized Pd–Ni core shell nanocrystal does self-assemble to yield well-ordered two-dimensional arrays [21]. A two-dimensional array obtained in the case of $Pd_{561}Ni_{561}$ array is shown in Fig. 8. All the arrays of the $Pd_{561}Ni_n$ nanocrystals are particularly well ordered, those with high Ni coverage showing a tendency to form multilayers or crystallites. Further, the ligand shell of the Pd–Ni nanocrystals could also be replaced with long-chain amines [22]. The amine-capped nanocrystals also form well-ordered two-dimensional arrays, but significant differences exist between lattices formed by amine- and thiol-capped nanocrystals, as illustrated for the case of $Pd_{561}Ni_{3000}$ nanocrystals covered with octylamine and octanethiol in Fig. 9. It is seen that the $Pd_{561}Ni_{3000}$ nanocrystals covered with dodecanethiol exhibit a distinct tendency to form multilayers, while the same nanocrystals when coated with an amine yield two-dimensional structure.

Multilayer assemblies using monothiols are generally fragile. Multilayer deposition of nanocrystals is best achieved by the sequential adsorption of dithiol molecules and metal nanocrystals of the desired size, by dipping the substrate into the respective solutions with intermediate steps involving
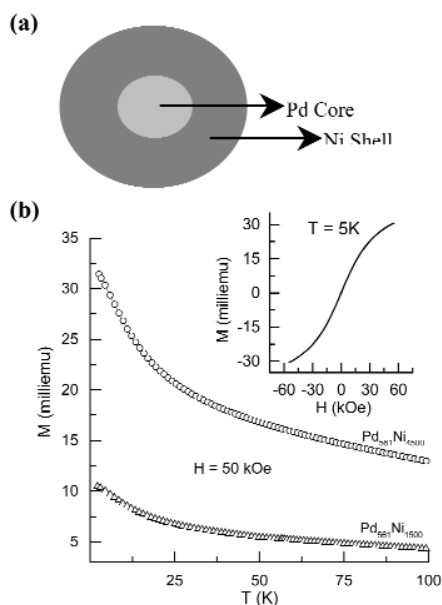
(a)

Pd Core
Ni Shell

(b)

Fig. 7 (a) A schematic illustration of the core-shell Pd–Ni nanocrystals. (b) Temperature dependence of magnetization for $Pd_{561}Ni_x$ core-shell nanocrystals with $x = 1500$ and 4500 under an applied field of 50 kOe. The values were corrected for contribution from the solvent and the glass tube. Inset shows the change in the magnetization (uncorrected) as a function of magnetic field for $x = 4500$ at 5 K.
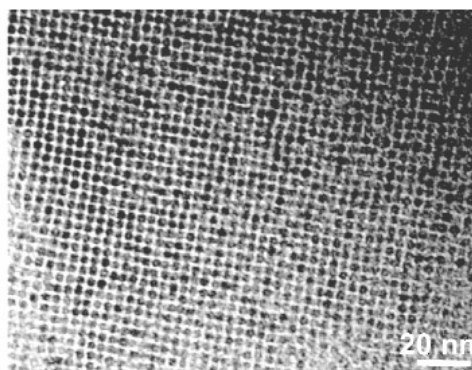

Fig. 8 TEM image of an ordered array of octanethiol capped $Pd_{561}Ni_{561}$ core-shell nanocrystals.

washing with toluene and drying. Using this procedure, several monometal, bimetal, and metal-semiconductor superlattices have been prepared [23]. After each deposition, the structure was characterized by STM, X-ray diffraction, as well as by XPS. Three-dimensional superlattices involving nanocrystals of different metals (e.g. Pt, Au) and of metals and semiconductors (e.g., Au, CdS) have also been prepared and characterized.
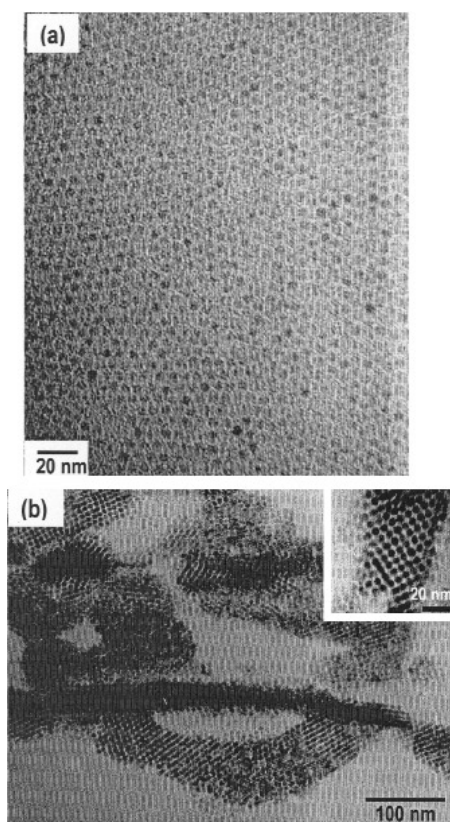
Fig. 9 TEM image showing arrays of $Pd_{561}Ni_{3000}$ nanocrystals coated with (a) octylamine and (b) octanethiol.

GIANT CLUSTERS OF MAGIC NUCLEARITY

It has been proposed that self-similarity in metal nanocrystal organization would manifest in the form of a giant cluster whose shape and size are direct consequences of the nanocrystals themselves [24]. The invariance of the shell effects in metal nanocrystals with scaling is shown schematically in Fig. 10. Thus, Pd_{561} nanocrystals would be expected to self-aggregate into a giant cluster of the type $(Pd_{561})_{561}$ under suitable conditions. Formation of such clusters was observed in the mass spectra of magic nuclearity Au_{55} nanocrystals. Secondary ion mass spectrometry indicated the presence of species with large m/z values, and these were attributed to $(Au_{13})_{55}$ giant clusters [25]. The giant clusters so obtained have, however, not been isolated or imaged. We made use of PVP-covered Pd_{561} nanocrystals in the study, since the monodisperse nature of the nanocrystals is important in assisting the self-aggregation process. When the PVP-covered Pd_{561} nanocrystals were allowed to stand in an aqueous medium, the particles aggregate to form giant clusters [26]. In Fig. 11a, we show a TEM image revealing the formation of the giant clusters. There are regions where the nanocrystals are densely packed in the form of aggregates. Importantly, the giant aggregates exhibit discrete sizes with diameters of 9.6, 15.6, 21.6, 33.8 nm. In order to calculate the number of nanocrystals in such a giant cluster, we first estimated the effective volume of a nanocrystal by measuring the shortest distance between nonaggregated particles. The mean value of this distance is 4.1 ($\sigma < 10$ %). This value is somewhat higher than the diameter estimated from STM (see Fig. 2) by ~0.5 nm. It is amazing that the estimated volume ratios show strong preference to the magic numbers. Thus, the nuclearity of the 9.6-nm giant cluster is 13 corresponding to the closure of first shell of nanocrystals. Similarly, the 15.6-nm giant cluster consists of 55 nanocrys-
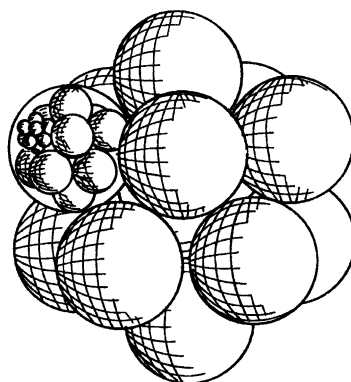
Fig. 10 Self-similarity: Schematic illustration of the formation of a cluster of metal nanocrystals (super cluster) and a cluster of superclusters. The size effects operating in nanocrystals could be invariant to scaling.
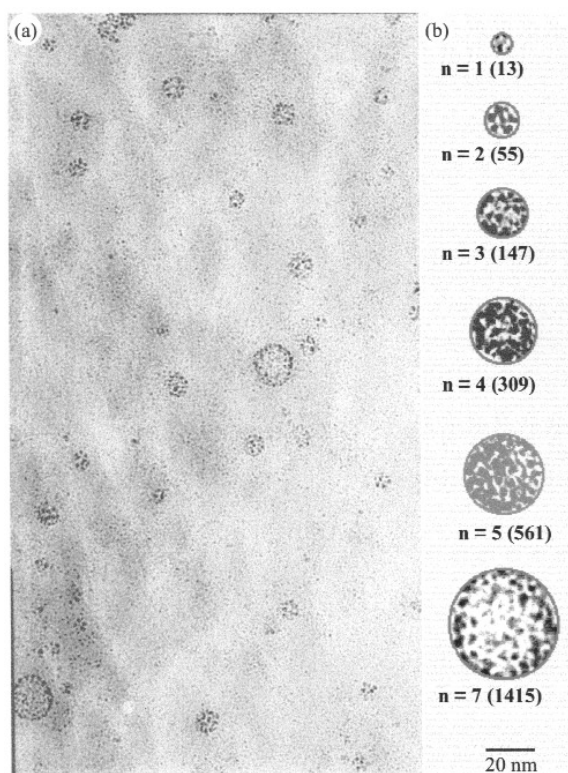

Fig. 11 (a) TEM micrograph showing the giant clusters comprising Pd_{561} nanocrystals. Sample for TEM was prepared by the slow evaporation of a PVP-Pd_{561} hydrosol. (b) Giant clusters enclosed in circles whose diameters correspond to magic numbers. The *n* values indicate the number of closed-shells. The values in parenthesis correspond to the number of Pd_{561} nanocrystals in the giant cluster.

tals in two closed-shells. Giant clusters of nanocrystals with nuclearities of 147 and 561 have also been observed. The giant clusters enclosed in the respective magic diameters are depicted in Fig. 11b. We find excellent agreement between the experimental diameters with those calculated from the effective

volume ratios. Images from the scanning electron microscope revealed the spherical shape of the giant clusters. We notice tiny spheres of ~10, 15, and 20 nm, corresponding to the magic nuclearity giant clusters. The spherical nature of the giant clusters was also confirmed by recording TEM images at various tilt angles. The individual Pd_{561} nanocrystals involved in the formation of giant clusters exhibit the characteristic lattice image, indicating thereby that the giant clusters truly consist of an assembly of distinguishable nanocrystals.

The giant clusters could be reproducibly formed starting from Pd_{561} nanocrystals in water, ethanol, and ethanol–water mixtures and from sols with very different concentrations of the nanocrystals. It is possible that the formation of the giant clusters is facilitated by the polymer shell that encases them. Unlike the case of Pd nanocrystals coated with alkanethiols, which self-assemble to form ordered arrays, the polymer shell effectively magnifies the facets of the metallic core, thereby aiding a giant assembly of the nanocrystals. The surface properties of the polymer-coated nanocrystals are clearly more favorable in that the interparticle interaction becomes sufficiently attractive.

CONCLUSIONS

Mesoscalar organization of metal nanocrystals has been discussed in this article. Thiolized metal nanocrystals self-assemble to give rise to hexagonal arrays. The nature of the organization depends on the particle diameter, d, and the alkane chain length l. Experimental observations on Pd nanocrystals relating the stability of the two-dimensional arrays to the d/l ratios find support from empirical calculations based on a soft sphere model. Nanocrystals with stabilization energies comparable to the thermal energy (few meV) give rise to close-packed hexagonal crystalline arrays whose d/l values are in the range 1.5–3.8. Large Pd nanocrystals ($d/l > 3$) with high stabilization energies (>10 meV) form collapsed structures while those attached to longer-chain thiols ($d/l \leq 1.5$) are associated with little stabilization, and exhibit low-order structures. The interparticle distances estimated from the soft-sphere model deviate to some extent from the experimental values owing to the interdigitation of thiol molecules chemisorbed on the curved nanocrystal surfaces. The extent of interdigitation of thiol shells, as well as the size distribution of particles, influence the quality of the organization. Three-dimensional arrangement of the nanocrystals, on the other hand, has been carried out on thiolized metal substrate by depositing layers of nanocrystals separated by dithiol spacers. Superlattices of Au and Pt nanocrystals, as well as heterostructures involving CdS particles, have been obtained in this fashion. Another example of the mesoscopic self-assembly of metal nanocrystals is the formation of giant clusters. PVP-protected Pd_{561} nanocrystals have been found to aggregate into giant clusters on removal of the solvent. The experimental observation that these clusters contain a magic number of nanocrystals makes the study very interesting.

REFERENCES

1. A. I. Kirkland, D. E. Jefferson, D. G. Duff, P. P. Edwards, I. Gameson, B. F. U. Johnson, D. J. Smith. *Proc. R. Soc. London. A* **440**, 589 (1993).
2. J. O. Bovin and J. O. Malm. *Z. Phys. D* **19**, 293 (1991).
3. T. P. Martin, T. Bergmann, H. Göhlich, T. Lange. *J. Phys. Chem.* **95**, 6421 (1991).
4. P. P. Edwards, R. L. Johnston, C. N. R. Rao. In *Metal Clusters in Chemistry*, P. Braunstein, G. Oro, P. R. Raithby (Eds.), Wiley-VCH, Weinheim (1999).
5. A. P. Alivisatos. *J. Phys. Chem. B* **100**, 13226 (1996).
6. C. N. R. Rao, G. U. Kulkarni, P. J. Thomas, P. P. Edwards. *Chem. Eur. J.* **29**, 8 (2002).
7. C. P. Vinod, G. U. Kulkarni, C. N. R. Rao. *Chem. Phys. Lett.* **289**, 329 (1998).
8. C. N. R. Rao, G. U. Kulkarni, P. John Thomas, P. P. Edwards. *Chem. Soc. Rev.* **29**, 27 (2000).
9. C. B. Murray, C. R. Kagan, M. G. Bawendi. *Science* **270**, 1335 (1995).
10. A. Terfort, N. Bowden, G. M. Whitesides. *Nature* **386**, 162 (1997).

11. C. A. Mirkin, R. L. Letsinger, R. C. Mucic, J. F. Storhoff. *Nature* **382**, 607 (1996).
12. B. A. Korgel and D. Fitzmaurice. *Phys. Rev. Lett.* **80**, 3531 (1998).
13. K. V. Sarathy, G. Raina, R. T. Yadav, G. U. Kulkarni, C. N. R. Rao. *J. Phys. Chem. B* **101**, 9876 (1997).
14. K. V. Sarathy, G. U. Kulkarni, C. N. R. Rao. *Chem. Commun.* 537 (1997).
15. P. J. Thomas, G. U. Kulkarni, C. N. R. Rao. *J. Phys. Chem. B* **104**, 8138 (2000).
16. R. J. Speedy. *J. Phys. Condens. Matter* **10**, 4185 (1998).
17. J. R. Heath, M. C. Knobler, D. V. Leff. *J. Phys. Chem. B* **101**, 189 (1997).
18. B. A. Korgel, S. Fullam, S. Connolly, D. Fitzmaurice. *J. Phys. Chem. B* **102**, 8379 (1998).
19. D. Bargeman and F. V. V. Vader. *J. Electroanal. Chem.* **37**, 45 (1972).
20. T. Teranishi and M. Miyake. *Chem. Mater.* **11**, 3414 (1999).
21. P. J. Thomas, G. U. Kulkarni, C. N. R. Rao. *J. Nanosci. Nanotechnol.* **1**, 267 (2001).
22. P. J. Thomas, P. Saravanan, G. U. Kulkarni, C. N. R. Rao. *Pramana—Journal of Physics* **58**, 371 (2002).
23. K. V. Sarathy, P. J. Thomas, G. U. Kulkarni, C. N. R. Rao. *J. Phys. Chem. B* **103**, 399 (1999).
24. H. G. Fritsche, H. Muller, B. Fehrensen. *Z. Phy. Chem.* **199**, 87 (1997).
25. H. Feld, A. Leute, D. Rading, A. Benninghoven, G. Schmid. *J. Am. Chem. Soc.* **112**, 8166 (1990).
26. P. J. Thomas, G. U. Kulkarni, C. N. R. Rao. *J. Phys. Chem. B* **105**, 2515 (2001).